Attosecond time delay in the photoionization of Mn in the region of the $3p \rightarrow 3d$ giant resonance

V. K. Dolmatov,[1] A. S. Kheifets,[2] P. C. Deshmukh,[3] and S. T. Manson[4]

[1]*Department of Physics and Earth Science, University of North Alabama, Florence, Alabama 35632, USA*

[2]*Research School of Physics and Engineering, The Australian National University, Canberra, ACT 0200, Australia*

[3]*Department of Physics, Indian Institute of Technology Madras, Chennai 600036, India*

[4]*Department of Physics and Astronomy, Georgia State University, Atlanta, Georgia 30303, USA*

(Received 15 December 2014; published 18 May 2015)

Initial insight into time delay in Mn photoionization in the region of the $3p \rightarrow, 3d$ giant autoionization resonance is gained in the framework of the "spin-polarized" random-phase approximation with exchange. The dramatic effect of the giant autoionization resonance on the time delay of photoemission from the $3d$ and $4s$ valence subshells of the Mn atom is unraveled. Strong sensitivity of the time delay of the $4s$ photoemission to the final-state term of the ion remainder [$Mn^+(4s^1, {}^5S)$ vs $Mn^+(4s^1, {}^7S)$] is discovered. It is shown that photoionization time delay in the autoionizing resonance region is explicitly associated with the resonance lifetime, which can thus be directly measured in attosecond time-delay experiments. Similar features are expected to emerge in photoionization time delays of other transition-metal and rare-earth atoms with half-filled subshells that possess giant autoionization resonances as well.

DOI: 10.1103/PhysRevA.91.053415 PACS number(s): 32.80.Fb, 32.80.Rm, 32.80.Zb, 42.50.Hz

I. INTRODUCTION

Atomic photoionization time delay is characterized by a slight temporal offset in the release of the photoelectron wave packet upon absorption of a short electromagnetic pulse by an atom. Since the first experimental and theoretical demonstration that atomic photoionization time delay can be measured using a single attosecond pulse (SAP) [1], it has become an active topic of investigation. A series of experiments was conducted recently using attosecond pulse trains (APTs) [2–6]. The experimental results thus produced were analyzed using several theoretical models of various degrees of sophistication [7–15]. At the same time, there exists a large body of literature on photoemission time delay in condensed matter, but reviewing this literature is outside the framework of the present article.

In essence, photoionization time delay is a direct generalization of the concept of time delay developed by Eisenbud [16] and Wigner [17] for electron scattering and applied recently to atomic photoionization in Ref. [1]. Normally, the delay is small, of the order of tens to hundreds of attoseconds (1 as $= 10^{-18}$ s). Experimental observation of this phenomenon allows one to capture electron motion in atoms, molecules, and solids on its natural, attosecond time scale. In turn, unique experimental accomplishments provide the impetus for advanced theoretical studies of the photoionization time-delay phenomenon as well.

Photoionization time delay has been studied in closed-shell systems like noble-gas atoms. However, it would also be interesting to study the photoionization time delay in transition-metal atoms. This was briefly addressed only for elastic electron scattering off Mn in [18]. Meanwhile, time delay in the photoemission spectra of transition-metal atoms presents an especially interesting case. Owing to the open-shell nature of the valence $nd^{q<10}$ subshells of these atoms ($n = 3$ for iron-group atoms, like the Mn atom), their photoionization spectra are dominated by the $np \rightarrow nd$ giant autoionization resonance which subsequently autoionizes into primarily $nd \rightarrow f, p$ channels. The $np \rightarrow nd$ giant resonance was originally detected experimentally in the $3p$ photoabsorption spectrum of Mn by Connerade *et al.* [19]. Later, it was experimentally and theoretically studied not only in Mn but in other transition-metal atoms and their ions (see review papers by Sonntag and Zimmermann [20] and Martins *et al.* [21], as well as references cited below in this paper).

It is the ultimate aim of the present study to get insight into the impact of the $3p \rightarrow 3d$ giant autoionization resonance in the Mn($[Ar]3d^5 4s^2, {}^6S$) atom on time delays in photoionization of the $3d$ and $4s$ valence subshells of the atom.

The effect of resonances on measuring and interpreting atomic photoemission time delay has been studied previously. In Ref. [22] doubly excited states of Ne were scrutinized to explain the discrepancy between experiment and theory reported in Ref. [1]. Similar attempts were made to reconcile the theory and experiment for photoemission time delay near the $3s$ Cooper minimum in Ar [23]. However, neither of these attempts was successful. In Ne, the resonances proved to be too narrow to have any effect on the measured time delay. In Ar, the latest and most accurate set of time delay results [24] was found to disagree with the theoretical predictions of [23].

There are reasons for choosing Mn for this study. First, $3d$ photoionization of neutral Mn in the region of the $3p \rightarrow 3d$ resonance was studied extensively experimentally [20,21,25–27]. Thus, Mn is well disposed for experimental photoionization measurements, and there is reliable experimental information to assess the quality of corresponding theoretical calculations. Second, Mn is not just an open-shell atom but a half-filled shell atom. This simplifies its theoretical study significantly. In particular, one can employ a multielectron "spin-polarized" random-phase approximation with exchange (SPRPAE) [28–30] designed especially to describe photoionization of half-filled shell atoms. Finally, SPRPAE has been successfully used to study the $3p \rightarrow 3d$ giant resonance in $3d$ [28] and $4s$ [31,32] photoionization of Mn, and good quantitative agreement with experiment [20,25,26] and many-body-perturbation theory (MBPT) theory [33] was achieved. Thus, SPRPAE is a convenient theoretical method for gaining the initial insight into time delays in Mn photoionization.

It is therefore chosen as the theoretical tool for the present study.

Atomic units are used throughout the paper unless otherwise specified.

II. REVIEW OF THEORY

A convenient starting point to account for the structure of a half-filled shell atom is provided by the spin-polarized Hartree-Fock (SPHF) approximation developed by Slater [34]. SPHF accounts for the fact that spins of all electrons in a half-filled subshell of the atom (e.g., in the $3d^5$ subshell of Mn) are aligned, say, pointing upward, in accordance with Hund's rule. This results in the splitting of a closed $n\ell^{2(2\ell+1)}$ subshell in the atom into two half-filled subshells of opposite spin orientations, $n\ell^{2\ell+1}\uparrow$ and $n\ell^{2\ell+1}\downarrow$. This is due to the presence of the exchange interaction between $n\ell\uparrow$ electrons with only spin-up electrons of a spin-unpaired half-filled subshell of the atom (e.g., the $3d^5\uparrow$ subshell in the Mn atom) but the absence of such interaction for $n\ell\downarrow$ electrons. Therefore, atoms with half-filled subshells can be treated as having only occupied subshells, filled in only by either one or the other kind of electrons, named "up" or "down" electrons depending on their spin orientations, $\uparrow$ and $\downarrow$, respectively [28,34]. Their binding energies $\epsilon_{n\ell\uparrow(\downarrow)}$ and wave functions $P_{\epsilon\uparrow(\downarrow)}(r)$ differ from each other, as is clear from the discussion above. They are solutions of the corresponding SPHF equations, which differ from the ordinary Hartree-Fock equations by accounting for exchange interactions only between electrons with the same spin orientation [30,34]. For the Mn atom, which is the atom of interest in the present paper, the SPHF configuration is $[\mathrm{Ar}]3p^3\uparrow 3p^3\downarrow 3d^5\uparrow 4s^1\uparrow 4s^1\downarrow$ ($^6S_{5/2}$). The removal of a $3d\uparrow$ electron produces the ion remainder $\mathrm{Mn}^+(3d^4\uparrow\ 4s^1\uparrow\ 4\mathrm{s}\downarrow, ^5D_4)$. A removal of a spin-up $4s\uparrow$ or spin-down $4s\downarrow$ electron from Mn results in ion remainders having different terms, the $\mathrm{Mn}^+(3d^5\uparrow 4s^1\downarrow, ^5S_2)$ and $\mathrm{Mn}^+(3d^5\uparrow 4s^1\uparrow, ^7S_3)$ ions, respectively. This makes the photoionization process spin dependent, or, in other words, term dependent. In the present paper, "term dependence" and "spin dependence" are used interchangeably.

The multielectron SPRPAE [28–30] utilizes SPHF as the zero-order independent-particle basis: the vacuum state. This is because the spin-up and spin-down subshells of the atom can be regarded as completely filled. Therefore, the well-developed random-phase approximation with exchange (RPAE) for closed-shell atoms [30] can be easily generalized to the case of half-filled-shell atoms. Similar to RPAE, the SPRPAE equation for a photoionization amplitude $\langle k|\hat{D}|i\rangle \equiv D_{ki}$ of the ith subshell of an atom into a continuous state k is depicted graphically in Fig. 1. Figures 1(c)–1(f) represent SPRPAE (RPAE) corrections to the HF photoionization amplitude $\langle k|\hat{d}|i\rangle \equiv d_{ik}$ [Fig. 1(b)]. Figures 1(d) and 1(f) account for the exchange interaction in the atom and are thus called the exchange diagrams. In SPRPAE, the contribution of the exchange diagrams [Figs. 1(d) and 1(f)] to the photoionization amplitude is discarded from the equation whenever the corresponding intermediate-state electron-hole pair j-k' and the final-state electron-hole pair i-k have opposite spin orientations. The exchange diagrams in Figs. 1(d) and 1(f), in fact, represent an infinite sum over all orders of perturbation theory in the interelectron interaction. Therefore, the presence of certain series of exchange diagrams in the SPRPAE equation for photoionization of an electron with one spin polarization (e.g., a spin-up electron) and the absence of this series of exchange diagrams in the corresponding equation for photoionization of an electron with an opposite spin orientation (spin-down electron, in this example) matter a lot. This enhances the photoionization term dependence of a half-filled-shell atom considerably compared to SPHF results. In fact, such term dependence was found to be dramatic not only for dipole photoionization of the outermost ns subshells in half-filled-shell atoms [31,32,35] but for nondipole photoionization as well [36].

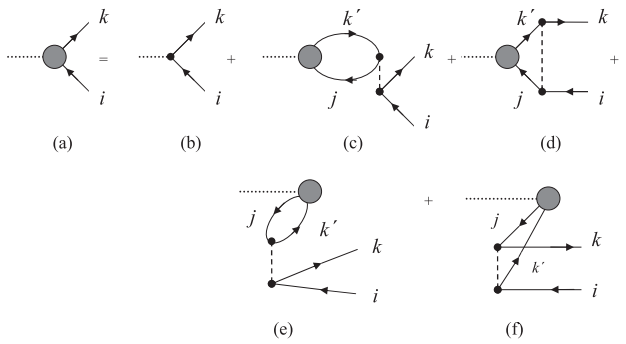

FIG. 1. Feynman diagrammatic representation of the SPRPAE (RPAE) equation for the photoionization amplitude $\langle k|\hat{D}|i\rangle$ of the ith subshell into the kth final state [30]. Here, the time axis is directed from the left to right, the lines with arrows to the left (right) correspond to holes (electrons) in the atom, a dotted line represents an incoming photon, a dashed line represents the Coulomb interaction $V(r)$ between charged particles, and a shaded circle marks the effective operator $\hat{D}$ for the photon-atom interaction which accounts for electron correlation in the atom.

We now briefly outline the key points of the photoionization time-delay concept. In the spirit of the Eisenbud-Wigner theory for time delay in electron scattering [16,17], time delay in the photoionization of an n_il_i subshell of the atom is determined by a derivative of the phase $\varphi(E)$ of the corresponding photoionization amplitude $T_{n_il_i} = |T_{n_il_i}|e^{i\varphi(E)}$ [37]. Correspondingly,

$$\varphi(E) = \arg[T_{n_il_i}(E)], \quad \tau_{n_il_i} = \frac{d\varphi(E)}{dE}. \tag{1}$$

For a photoionization amplitude $T_{n_il_i}$ of a n_il_i state which accounts for both $n_il_i \to \epsilon(l_i \pm 1)$ dipole transitions, one has [15]

$$T_{n_il_i}(E) \propto \sum_{\substack{l=l_i\pm1\\ m=m_i}} e^{i\delta_l} i^{-l} Y_{lm}(\hat{\boldsymbol{k}})\,(-1)^m \begin{pmatrix} l & 1 & l_i \\ -m & 0 & m_i \end{pmatrix} \times \langle El\|D\|n_il_i\rangle. \tag{2}$$

Here, $\hat{\boldsymbol{k}}$ is a unit vector in the direction of the photoelectron momentum $\boldsymbol{k}$, $\delta_l(E)$ is the phase shift of the lth outgoing photoelectron wave, and $\langle El\|D\|n_il_i\rangle$ is the reduced dipole matrix element which is the solution of the RPAE (or SPRPAE in our work) equation (Fig. 1). Since the matrix element $T_{n_il_i}$ defined by Eq. (2) depends on the photoelectron emission

angles, it will be referred to, when emphasis is needed, as the angle-dependent matrix element. In the present work, $T_{n_i l_i}(E)$ is evaluated in the forward direction $\boldsymbol{k} \| \hat{z}$, which is usually the case in the attosecond time-delay measurements; this is of importance because the time delay, in general, has an angular dependence [38,39].

Summarizing the review of theory, the Eisenbud-Wigner time delay (1) is defined by the complex phase of the stationary ionization amplitude corresponding to a given energy of the ionizing field ω. However, in SAP or APT measurements, time delay is determined by a combination of the ionizing field and the streaking probe that is used. This introduces the so-called Coulomb-laser coupling corrections [9] (SAP) or continuum-continuum corrections [12] (APT). The latter reference also demonstrated the equivalence of the corrections in the SAP and APT measurements. In nonresonant photoionization, these corrections should be added to the Eisenbud-Wigner time delay to account for the experimentally measured time delay.

In resonant photoionization, the effect of the measurement on the Eisenbud-Wigner time delay is much more complicated. Indeed, the SAP measurement involves an attosecond pulse of considerable bandwidth which is required to be much larger than the photon energy of the probing pulse $\Omega \simeq 1.5$ eV [12]. Such wide spectral bandwidth could, at least partially, "mask" an autoionization resonance of comparable width which is manifested in the present Mn $3p \rightarrow 3d$ case, so it might be difficult to employ the SAP technique to verify the predictions. On the other hand, although the APT technique is free from the bandwidth limitations, the usual two-frequency modulation of the two-photon interference is strongly distorted by the presence of an autoionizing resonance [40]. Hence, a more involved analysis is required that cannot be reduced to adding a unified set of the continuum-continuum corrections. Recently, an analysis was provided by a general analytical model that accounts for the effect of both intermediate and final resonances on two-photon processes [40]. With the helium atom as the case study, this analysis yielded the same result as a solution of the all-dimensional time-dependent Schrödinger equation. Therefore, the APT technique appears to be more suitable than SAP to address a resonance problem, although it is not entirely clear how it could account for the interchannel interference.

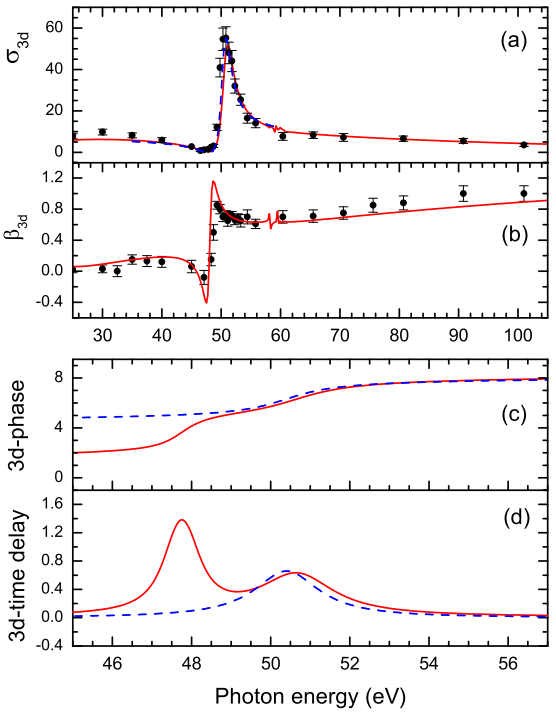

FIG. 2. (Color online) (a) Solid line: present calculated SPRPAE data for the Mn $3d \uparrow$ photoionization cross sections σ_{3d} (in units of megabarns); dots: experimental data on an absolute scale taken from Table 3 of Ref. [25]; dashed line: SPRPAE σ_{3d} calculated previously [28] on the basis of the Fano autoionization formalism in the region of the $3p \downarrow \rightarrow 3d \downarrow$ giant resonance. (b) Solid line: present calculated SPRPAE angular-asymmetry parameter β_{3d}; dots: experimental data from Table 3 of Ref. [25]. (Note that former SPRPAE results for β_{3d} [28], obtained on the basis of the Fano formalism in the region of the $3p \downarrow \rightarrow 3d \downarrow$ giant resonance, practically coincide with the present data and are not plotted). (c) Solid line: calculated SPRPAE phase $\varphi_{3d}(\omega)$ (in units of radians) of the $3d \uparrow$ photoionization amplitude T_{3d} [Eq. (2)]; dashed line: the same as above but calculated with the help of the single-channel Fano formula [Eq. (3)]. (d) Solid line: calculated SPRPAE time delay $\tau_{3d}(\omega)$ (in units of femtoseconds); dashed line: $\tau_{3d}(\omega)$ calculated with the help of the single-channel Fano formula [Eq. (4)].

III. RESULTS AND DISCUSSION

A. Mn 3*d* photoionization

The SPRPAE calculations of Mn $3d$ photoionization in the region of the $3p \downarrow \rightarrow 3d \downarrow$ giant autoionization resonance were performed while including interchannel coupling among four ($3d \uparrow \rightarrow f \uparrow$, $3d \uparrow \rightarrow p \uparrow$, $3p \downarrow \rightarrow d \downarrow$, and $3p \downarrow \rightarrow s \downarrow$) transitions. Interchannel coupling with other transitions was considered negligible and was ignored. Next, calculated SPHF values for the ionization potentials $I_{3d\uparrow} \approx 17.4$ eV and $I_{3p\downarrow} \approx 60.7$ eV, as well as binding energies of discrete excitations, were used in this calculation because the use of HF (SPHF) ionization potentials is conceptually consistent with RPAE (SPRPAE) theory. Moreover, earlier [28], the use of SPHF ionization thresholds in the calculated SPRPAE $3d$ photoionization cross section of Mn in the region of the $3p \rightarrow 3d$ resonance was shown to result in good agreement between theory and experiment.

The present calculated SPRPAE results for the $3d \uparrow$ photoionization cross section $\sigma_{3d}(\omega)$ and $3d$ angular-asymmetry parameter β_{3d} (refer, e.g., to Ref. [30] for the equations for σ_{nl} and β_{nl}) are plotted in Figs. 2(a) and 2(b) between 25 and 105 eV along with corresponding experimental data from Ref. [25]. One can see reasonable agreement between theory and experiment not only for $\sigma_{3d}(\omega)$ but for β_{3d} as well. The angular-asymmetry parameter β_{3d} depends not only on the absolute values of the photoionization amplitudes but also on phase shifts of the amplitudes. Therefore, reasonable agreement between the present calculated SPRPAE data and experiment for β_{3d} is indicative of reasonably correctly calculated phases of the photoionization matrix elements and thus $3d$ time delay τ_{3d} as well. The calculated SPRPAE phase $\varphi_{3d}(\omega)$ and time delay $\tau_{3d}(\omega)$ in the region of the

$3p \downarrow \rightarrow 3d \downarrow$ giant resonance are depicted in Figs. 2(c) and 2(d), respectively.

Note also how significantly the region of the giant resonance impacts both $\varphi_{3d}(\omega)$ and $\tau_{3d}(\omega)$ compared to the region away from the resonance. Specifically, the giant resonance enhances the time delay $\tau_{3d}(\omega)$ by more than one order of magnitude compared to its nonresonance value, at both $\omega \approx 48$ and 50.5 eV. It is important to note that the latter enhancement of $\tau_{3d}(\omega)$ occurs in the photon energy region where the cross section is large, $\sigma_{3d} \approx 55$ Mb. This should facilitate greatly its experimental observation.

It is also instructive to make a simple evaluation of a photoionization amplitude T_{3d}, its phase φ_{3d}, and time delay τ_{3d} in the region of the $3p \downarrow \rightarrow 3d \downarrow$ giant resonance within the framework of the Fano theory [41]. Single-channel, single-resonance parametric expressions for the generally dominant matrix element $T_{3d\rightarrow f}(\omega) \equiv T$ [Eq. (2)] and the photoionization cross section $\sigma_{3d\rightarrow f}(\omega) \equiv \sigma$ read

$$T(\omega) = T_0 \frac{q+\epsilon}{i+\epsilon}, \quad \sigma(\omega) = \sigma_0 \frac{(q+\epsilon)^2}{1+\epsilon^2}, \quad \epsilon = \frac{\omega - \omega_r}{\gamma/2}. \tag{3}$$

Here, T_0 and σ_0 are, respectively, the $3d \uparrow \rightarrow f \uparrow$ photoionization amplitude and cross section calculated without accounting for the $3p \downarrow \rightarrow 3d \downarrow$ resonance transition, ω_r is the resonance energy, q is the profile index (shape parameter), and γ is the resonance width. In Mn, calculated SPRPAE $\gamma \approx 2$ eV, $\omega_r \approx 50.4$ eV, $q \approx 2.5$, and $\sigma_0 \approx 7.6$ Mb [28].

With the help of Eqs. (1) and (3) one finds that the time delay $\tau_{3d\rightarrow f}$ in a single-resonance, single-channel photoionization Fano formalism is determined as follows:

$$\tau_{3d\rightarrow f}(\omega) = \frac{2}{\gamma} \frac{1}{1+\epsilon^2}. \tag{4}$$

It follows from Eq. (4) that single-channel, single-resonance time delay has only one maximum which emerges at $\epsilon = 0$, i.e., at the resonance energy $\omega = \omega_r$. Moreover, one readily finds from Eq. (4) that the resonance width $\gamma = 2/\tau_{\max}$. The important implication is that the resonance width γ at the half maximum of the photoionization cross section is explicitly defined by $\tau_{\max}$. This opens a unique possibility for measuring the autoionization resonance lifetime directly in attosecond time-delay experiments, similar to the corresponding direct measurement of the Kr $3p$ vacancy Auger decay lifetime [42]. Furthermore, it is clear from the above that time delay in the autoionization resonance energy region reaches its maximum where the photoionization cross section $\sigma_{nl} = q^2\sigma_0$. One then concludes that the photoionization time delay is easier to measure in regions of autoionization resonances with large profile indices q.

The cross section $\sigma_{3d\rightarrow f}$, the phase $\varphi_{3d\rightarrow f}$, and the time delay $\tau_{3d\rightarrow f}$ calculated within the framework of the Fano formalism, discussed above, are depicted in Fig. 2. They are in a close agreement with the calculated SPRPAE data except for a region near 48 eV. There, the calculated SPRPAE time delay τ_{3d} has a strong resonance structure where τ_{3d} steeply rises to more than 1.5 fs below 48 eV. This resonance is then followed by a broader resonance in τ_{3d} at higher energies where τ_{3d} reaches about 0.6 fs near the maximum of σ_{3d} at $\omega \approx 50.5$ eV; the latter is in agreement with the Fano formalism.

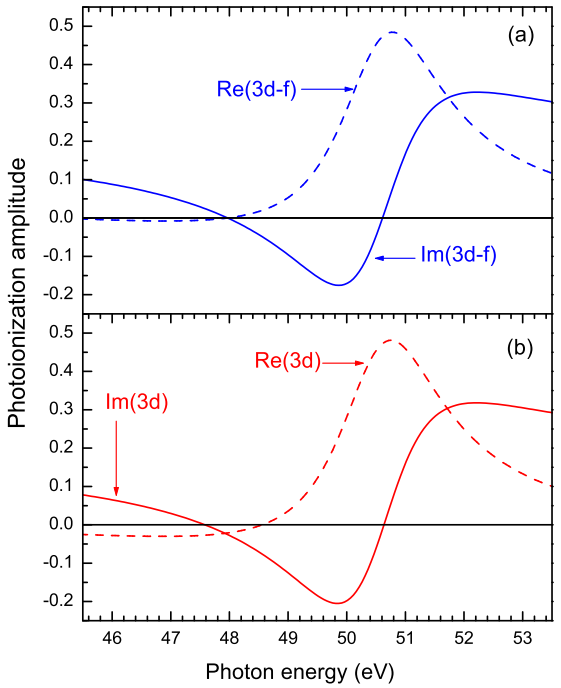

FIG. 3. (Color online) (a) SPRPAE real ($\mathrm{Re}T_{3d\rightarrow f}$) and imaginary ($\mathrm{Im}T_{3d\rightarrow f}$) parts (in atomic units) of the dominant $T_{3d\rightarrow f}$ photoionization amplitude [Eq. (2)], calculated in the region of the giant $3p \downarrow \rightarrow 3d \downarrow$ resonance. (b) SPRPAE real ($\mathrm{Re}T_{3d}$) and imaginary ($\mathrm{Im}T_{3d}$) parts (in atomic units) of the total amplitude T_{3d}, calculated as the weighted sum of the two matrix elements $\langle Ef\|D\|3d\rangle$ and $\langle Ep\|D\|3d\rangle$ [Eq. (2)] in the region of the giant $3p \downarrow \rightarrow 3d \downarrow$ resonance.

In order to get insight into the reason for the emergence of the strong 48 eV resonance in τ_{3d} but the absence of such in $\tau_{3d\rightarrow f}$, we plot in Fig. 3 the real and imaginary parts of the corresponding two-channel-weighted photoionization amplitude $T_{3d}(\omega)$ along with those of the amplitude $T_{3d\rightarrow f}(\omega)$. One can see from Fig. 3 that, near 48 eV, the relative behavior of $\mathrm{Re}T_{3d\rightarrow f}$ and $\mathrm{Im}T_{3d\rightarrow f}$ of the partial $T_{3d\rightarrow f}$ amplitude is quite different than the relative behavior of $\mathrm{Re}T_{3d}$ and $\mathrm{Im}T_{3d}$ of the total amplitude T_{3d}. Indeed, $\mathrm{Re}T_{3d\rightarrow f}$ and $\mathrm{Im}T_{3d\rightarrow f}$ take the zero values simultaneously, i.e., at the same energy $\omega \approx 48$ eV, so their ratio and, thus, partial $\phi_{3d\rightarrow f}$ and $\tau_{3d\rightarrow f}$ remain about constant through 48 eV. In contrast, the zeros of $\mathrm{Re}T_{3d}$ and $\mathrm{Im}T_{3d}$ are separated from each other by an energy interval of about 1 eV, inside of which $\mathrm{Re}T_{3d}$ and $\mathrm{Im}T_{3d}$ take equal values at $\omega \approx 48$ eV. This causes a clear variation, which appears to be resonant, in $\tan\varphi(\omega)$ and thus in the phase $\varphi(\omega)$ and time delay $\tau_{3d}(\omega)$ as well. As a result, $\tau_{3d}(\omega)$ possesses the additional strong 48 eV resonance, but $\tau_{3d\rightarrow f}(\omega)$ does not. This finding is both interesting and important since it reveals the necessity for accounting for both generally dominant ($3d \rightarrow f$) and generally weaker ($3d \rightarrow p$) transitions in photoionization time-delay calculations.

B. Mn 4*s* photoionization

In this calculation, we use the experimental values [20] $I_{3d\uparrow}(^5D_4) = 14.301$ eV (versus $I^{\mathrm{SPHF}}_{3d\uparrow} = 17.43$ eV), $I_{4s\uparrow}(^5S) =$

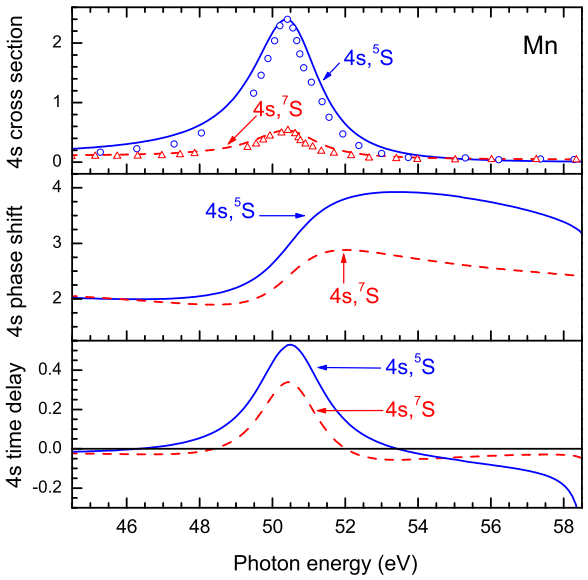

FIG. 4. (Color online) Calculated SPRPAE (present work) and experimentally measured [26] (open circles and triangles) Mn 4s photoionization cross sections (in units of megabarns) $\sigma_{4s\uparrow}(^5S)$ and $\sigma_{4s\downarrow}(^7S)$, as well as calculated SPRPAE phase shifts (in units of radians) $\varphi_{4s\uparrow}(^5S)$ and $\varphi_{4s\downarrow}(^7S)$ of the corresponding photoionization amplitudes [Eq. (2)] and time delays (in units of femtoseconds) $\tau_{4s\uparrow}(^5S)$ and $\tau_{4s\downarrow}(^7S)$, as marked. Relative experimental data [26] were normalized to the maxima in the calculated SPRPAE $\sigma_{4s\uparrow}(^5S)$ and $\sigma_{4s\downarrow}(^7S)$ and were shifted by 0.28 eV towards higher energies to match the position of the maxima in the calculated cross sections.

8.611 eV (versus $I^{\rm SPHF}_{4s\uparrow} = 7.44$ eV), and $I_{4s\downarrow}(^7S) = 7.431$ eV (versus $I^{\rm SPHF}_{4s\downarrow} = 6.15$ eV). This is because the 4$s\uparrow$ and 4$s\downarrow$ subshells of the Mn atom are significantly closer, in terms of energy, to the multielectron $3d^5\uparrow$ subshell than predicted by the SPHF theory. The use of the calculated SPHF ionization potentials in this case would have resulted in an underestimated coupling between the 4s and 3d ionization channels. Note that, as in the above case of the 3d photoionization, the calculated SPRPAE data for the 4s photoionization amplitudes were obtained with a direct solution of the SPRPAE equations, in contrast to work [31,32] where a Fano single-resonance formalism was exploited.

Results of the present SPRPAE calculation of $\sigma_{4s\uparrow}(^5S)$, $\sigma_{4s\downarrow}(^7S)$, $\varphi_{4s\uparrow}(^5S)$, and $\varphi_{4s\downarrow}(^7S)$, as well as $\tau_{4s\uparrow}(^5S)$ and $\tau_{4s\downarrow}(^7S)$, are depicted in Fig. 4. Note the good agreement between experiment and theory for $\sigma_{4s\uparrow}(^5S)$ and $\sigma_{4s\downarrow}(^7S)$. Furthermore, note how the time delays $\tau_{4s\uparrow}(^5S)$ and $\tau_{4s\downarrow}(^7S)$ are dramatically increased in the resonance region. Next, note how $\tau_{4s\uparrow}(^5S)$ and $\tau_{4s\downarrow}(^7S)$ differ strongly from each other in this energy region, where $\tau_{4s\uparrow}(^5S)$ exceeds $\tau_{4s\downarrow}(^7S)$ everywhere below an energy of $\omega \approx 54.7$ eV; above this energy the situation changes to the opposite. It is also interesting to note that $\tau_{4s\uparrow}(^5S)$ and $\tau_{4s\downarrow}(^7S)$ differ from each other strongly not only in magnitude but by sign as well, depending on ω. The noted differences between $\tau_{4s\uparrow}(^5S)$ and $\tau_{4s\downarrow}(^7S)$ constitute an interesting finding of a strong term dependence of time delay in 4s photoionization of Mn. This is due to SPRPAE exchange diagrams in Figs. 1(d) and 1(f), which contribute differently to photoionization of the 4$s\uparrow$ electron and photoionization of the 4$s\downarrow$ electron. For instance (see Fig. 1), if the intermediate excitation j-$k' \equiv 3d\uparrow \rightarrow \epsilon l\uparrow$, then the exchange diagrams [Figs. 1(d) and 1(f)] affect photoionization of a 4$s\uparrow$ electron but not a 4$s\downarrow$ electron (otherwise, the Coulomb interaction would have caused a spin-flip transition). Alternatively, Figs. 1(d) and 1(f) do not affect the 4$s\uparrow$ electron but do affect the 4$s\downarrow$ photoionization amplitude when j-$k' \equiv 3p\downarrow \rightarrow 3d\downarrow$. Thus, in the region of the $3p\downarrow \rightarrow 3d\downarrow$ giant resonance, where the impact of interchannel coupling of the $3p\downarrow \rightarrow 3d\downarrow$ and $3d\uparrow \rightarrow p\uparrow$, $f\uparrow$ channels with each of the $4s\uparrow \rightarrow p\uparrow$ and $4s\downarrow \rightarrow p\downarrow$ channels is significant, time delay in the 4s photoionization of Mn becomes strongly term dependent. This should be a general feature of other transition-metal atoms and ions as well.

IV. CONCLUSION

It has been demonstrated in this paper that time delays of the corresponding Mn 3d and 4s photoionization channels are dramatically increased in the region of the $3p \rightarrow 3d$ giant autoionization resonance. Furthermore, by utilizing the Fano formalism, it has been shown that the photoionization time delay in the autoionization resonance region is explicitly associated with the resonance lifetime. The latter can thus be determined directly from results of attosecond time-delay experiments. Furthermore, it has been found that the time delay of the 4s photoionization channel is strongly term dependent, resulting in significant differences between time delays $\tau_{4s\uparrow}(^5S)$ and $\tau_{4s\downarrow}(^7S)$. Strong maxima in $\tau_{3d\uparrow}(^4D)$, $\tau_{4s\uparrow}(^5S)$, and $\tau_{4s\downarrow}(^7S)$ emerge at photon energies where the corresponding photoionization cross sections are large, particularly for 3d photoionization. This should simplify experimental measurements of the phenomena described in Mn. Moreover, the $3p \rightarrow 3d$ giant autoionization resonance is known to occur in the photoabsorption spectra of Mn^+, metallic Mn, molecular $MnCl_2$, and solid $MnCl_2$ as well [43,44]. This provides the flexibility for experimental verification of the predictions made in this paper. It is expected that the features unraveled in time delays of the Mn photoelectron emission channels will emerge in other 3d and 4d transition elements and rare-earth elements where giant autoionization resonances exist as well. In other words, the features of time delays in Mn photoionization unveiled in the present paper are, in fact, inherent properties of not only the Mn atom in particular but other transition-metal and rare-earth atoms in general. Correspondingly, the results of the present paper provide guidance into photoionization time delays in those atoms as well.

Next, it is important to note that the well-known giant resonance in 4d photoionization of Xe (see, e.g., Ref. [30]) has found an important application in the induction of a strong enhancement of the high-order-harmonic generation (HHG) process [45]. The autoionization multielectron dynamics can be probed by the HHG technique [46] as well, particularly in the $3p \rightarrow 3d$ giant resonance in Mn, as shown by the large value of the Mn 3d photoionization cross section in recent work by Ganeev *et al.* [47]; the Mn 3d photoionization cross section is even greater than the Xe 4d photoionization cross section. Although experiments with metal vapors and ablation plasmas may be more challenging than those with noble gases, HHG experiments can now be performed [48] and analyzed [49]

in the condensed-matter phase. Solid-state Mn is a promising target for such a study.

In conclusion, it would be interesting to study how accounting for a large number of other open channels in the region of the Mn $3p \rightarrow 3d$ giant resonance, omitted in our SPRPAE study, could modify the predicted gross features in $3d$ and $4s$ time delays in this atom (apparently, it does not significantly modify the calculated SPRPAE σ_{3d} or β_{3d} in Mn). Our expectation is that possible alterations will not be drastic, but in the absence of experiment or other theoretical calculations related to this subject the question basically remains open. In fact, we consider the photoionization time-delay phenomenon in highly correlated atoms a unique touchstone for finer testing of existing and to-be-developed many-body theories against experiment. We urge the development of such calculations and experiments, and we hope that the initial insight into time delay in the Mn photoionization provided in the present paper serves as the impetus for such development.

ACKNOWLEDGMENTS

The authors are grateful to Dr. V. Yakovlev for his interest in this study. Dr. J. Jose is thanked for his assistance with the calculations. V.K.D. acknowledges the support of the NSF under Grant No. PHY-1305085. S.T.M. acknowledges the support of the Chemical Sciences, Geosciences and Biosciences Division, Office of Basic Energy Sciences, Office of Science, US Department of Energy under Grant No. DE-FG02-03ER15428. P.C.D. appreciates the support of the grant from the Department of Science and Technology, government of India.

[1] M. Schultze *et al.*, Delay in photoemission, Science **328**, 1658 (2010).

[2] K. Klünder, J. M. Dahlström, M. Gisselbrecht, T. Fordell, M. Swoboda, D. Guénot, P. Johnsson, J. Caillat, J. Mauritsson, A. Maquet, R. Taïeb, and A. L'Huillier, Probing single-photon ionization on the attosecond time scale, Phys. Rev. Lett. **106**, 143002 (2011).

[3] D. Guénot, K. Klünder, C. L. Arnold, D. Kroon, J. M. Dahlström, M. Miranda, T. Fordell, M. Gisselbrecht, P. Johnsson, J. Mauritsson, E. Lindroth, A. Maquet, R. Taïeb, A. L'Huillier, and A. S. Kheifets, Photoemission-time-delay measurements and calculations close to the $3s$-ionization-cross-section minimum in Ar, Phys. Rev. A **85**, 053424 (2012).

[4] D. Guénot, D. Kroon, E. Balogh, E. W. Larsen, M. Kotur, M. Miranda, T. Fordell, P. Johnsson, J. Mauritsson, M. Gisselbrecht, K. Varjú, C. L. Arnold, T. Carette, A. S. Kheifets, E. Lindroth, A. L'Huillier, and J. M. Dahlström, Measurements of photoemission time delays in noble gas atoms, J. Phys. B **47**, 245602 (2014).

[5] C. Palatchi, J. M. Dahlström, A. S. Kheifets, I. A. Ivanov, D. M. Canaday, P. Agostini, and L. F. DiMauro, Atomic delay in helium, neon, argon and krypton, J. Phys. B **47**, 245003 (2014).

[6] S. B. Schoun, R. Chirla, J. Wheeler, C. Roedig, P. Agostini, L. F. DiMauro, K. J. Schafer, and M. B. Gaarde, Attosecond pulse shaping around a Cooper minimum, Phys. Rev. Lett. **112**, 153001 (2014).

[7] A. S. Kheifets and I. A. Ivanov, Delay in atomic photoionization, Phys. Rev. Lett. **105**, 233002 (2010).

[8] L. R. Moore, M. A. Lysaght, J. S. Parker, H. W. van der Hart, and K. T. Taylor, Time delay between photoemission from the $2p$ and $2s$ subshells of neon, Phys. Rev. A **84**, 061404 (2011).

[9] S. Nagele, R. Pazourek, J. Feist, K. Doblhoff-Dier, C. Lemell, K. Tökési, and J. Burgdörfer, Time-resolved photoemission by attosecond streaking: extraction of time information, J. Phys. B **44**, 081001 (2011).

[10] J. M. Dahlström, T. Carette, and E. Lindroth, Diagrammatic approach to attosecond delays in photoionization, Phys. Rev. A **86**, 061402 (2012).

[11] J. M. Dahlström, A. L'Huillier, and A. Maquet, Introduction to attosecond delays in photoionization, J. Phys. B **45**, 183001 (2012).

[12] J. Dahlström, D. Guénot, K. Klünder, M. Gisselbrecht, J. Mauritsson, A. L. Huillier, A. Maquet, and R. Taïieb, Theory of attosecond delays in laser-assisted photoionization, Chem. Phys. **414**, 53 (2013).

[13] A. S. Kheifets, Time delay in valence-shell photoionization of noble-gas atoms, Phys. Rev. A **87**, 063404 (2013).

[14] J. Feist, O. Zatsarinny, S. Nagele, R. Pazourek, J. Burgdörfer, X. Guan, K. Bartschat, and B. I. Schneider, Time delays for attosecond streaking in photoionization of neon, Phys. Rev. A **89**, 033417 (2014).

[15] S. Saha, A. Mandal, J. Jose, H. R. Varma, P. C. Deshmukh, A. S. Kheifets, V. K. Dolmatov, and S. T. Manson, Relativistic effects in photoionization time delay near the Cooper minimum of noble-gas atoms, Phys. Rev. A **90**, 053406 (2014).

[16] L. Eisenbud, Formal properties of nuclear collisions, Ph.D. thesis, Princeton University (1948).

[17] E. P. Wigner, Lower limit for the energy derivative of the scattering phase shift, Phys. Rev. **98**, 145 (1955).

[18] V. K. Dolmatov, M. Ya. Amusia, and L. V. Chernysheva, Electron elastic scattering off a semifilled-shell atom: The Mn atom, Phys. Rev. A **88**, 042706 (2013).

[19] J. P. Connerade, M. W. D. Mansfield, and M. A. P. Martin, Observation of a giant resonance in the 3p absorption spectrum of Mn I, Proc. R. Soc. London, Ser. A **350**, 405 (1976).

[20] B. Sonntag and P. Zimmermann, XUV spectroscopy of metal atoms, Rep. Prog. Phys. **55**, 911 (1992).

[21] M. Martins, K. Godehusen, T. Richter, P. Wernet, and P. Zimmermann, Open shells and multi-electron interactions: core level photoionization of the 3d metal atoms, J. Phys. B **39**, R79 (2006).

[22] Y. Komninos, Th. Mercouris, and C. A. Nicolaides, Regular series of doubly excited states inside two-electron continua: Application to $2s^2$-hole states in neon, above the $Ne^{2+}1s^22s^22p^4$ and $1s^22s2p^5$ thresholds, Phys. Rev. A **83**, 022501 (2011).

[23] T. Carette, J. M. Dahlström, L. Argenti, and E. Lindroth, Multiconfigurational Hartree-Fock close-coupling ansatz:

Application to the argon photoionization cross section and delays, Phys. Rev. A **87**, 023420 (2013).

[24] M. Sabbar, S. Heuser, R. Boge, M. Lucchini, T. Carette, E. Lindroth, L. Gallmann, C. Cirelli, and U. Keller, Resonance effects in photoemission time delays, arXiv:1407.6623.

[25] M. O. Krause, T. A. Carlson, and A. Fahlman, Photoelectron spectrometry of manganese vapor between 12 and 110 eV, Phys. Rev. A **30**, 1316 (1984).

[26] S. B. Whitfield, M. O. Krause, P. van der Meulen, and C. D. Caldwell, High-resolution photoelectron spectrometry of atomic manganese from the region of the $3p \rightarrow 3d$ giant resonance to 120 eV, Phys. Rev. A **50**, 1269 (1994).

[27] T. Osawa, K. Kawajiri, N. Suzuki, T. Nagata, Y. Azuma, and F. Koike, Photoion-yield study of the $3p - 3d$ giant resonance excitation region of isolated Cr, Mn and Fe atoms, J. Phys. B **45**, 225204 (2012).

[28] M. Ya. Amus'ya, V. K. Dolmatov, and V. K. lvanov, Photoionization of atoms with half-filled shells, Sov. Phys. JETP **58**, 67 (1983).

[29] M. Ya. Amusia and V. K. Dolmatov, Photoionization of inner ns electrons in semifilled shell atoms (3*s* electrons in a Mn atom), J. Phys. B **26**, 1425 (1993).

[30] M. Ya. Amusia and L. V. Chernysheva, *Computation of Atomic Processes: A Handbook for the ATOM Programs* (Institute of Physics, Bristol, UK, 1997).

[31] M. Ya. Amusia, V. K. Dolmatov, and V. M. Romanenko, Exchange electron correlation effects in outer-level photoionisation of half-filled subshell atoms (Mn), J. Phys. B. **21**, L151 (1988).

[32] M. Ya. Amusia, V. K. Dolmatov, and M. M. Mansurov, A new feature of the $3p \rightarrow 3d$ transition in the Mn atom, J. Phys. B **23**, L491 (1990).

[33] L. J. Garvin, E. R. Brown, S. L. Carter, and H. P. Kelly, Calculation of photoionisation cross sections, resonance structure and angular distribution for Mn I by many-body perturbation theory, J. Phys. B **16**, L269 (1983).

[34] J. C. Slater, *The Self-Consistent Field for Molecules and Solids* (McGraw-Hill, New York, 1974).

[35] V. K. Dolmatov and M. M. Mansurov, Trends in valence autoionizing Rydbergs for nd^5 semifilled-shell ground and excited atoms and ions: Cr, Mn, Mn^+, Fe^+, Fe^{2+}, Mo, Tc, Tc^+ and Re, J. Phys. B **29**, L307 (1996).

[36] V. K. Dolmatov and S. T. Manson, Strong final-state term dependence of nondipole photoelectron angular distributions from half-filled shell atoms, Phys. Rev. A **74**, 032705 (2006).

[37] F. T. Smith, Lifetime matrix in collision theory, Phys. Rev. **118**, 349 (1960).

[38] J. Wätzel, A. S. Moskalenko, Y. Pavlyukh, and J. Berakdar, Angular resolved time delay in photoemission, J. Phys. B **48**, 025602 (2015).

[39] J. M. Dahlström and E. Lindroth, Study of attosecond delays using perturbation diagrams and exterior complex scaling, J. Phys. B **47**, 124012 (2014).

[40] A. Jiménez-Galán, L. Argenti, and F. Martín, Modulation of attosecond beating in resonant two-photon ionization, Phys. Rev. Lett. **113**, 263001 (2014).

[41] U. Fano, Effects of configuration interaction on intensities and phase shifts, Phys. Rev. **124**, 1866 (1961).

[42] M. Drescher, M. Hentschel, R. Kienberger, M. Uiberacker, V. Yakovlev, A. Scrinzi, T. Westerwalbesloh, U. Kleineberg, U. Heinzmann, and F. Krausz, Time-resolved atomic inner-shell spectroscopy, Nature (London) **419**, 803 (2002).

[43] B. Sonntag, R. Haensel, and C. Kunz, Optical absorption measurements of the transition metals Ti, V, Cr, Mn, Fe, Co, Ni in the region of 3p electron transitions, Solid State Commun. **7**, 597 (1969).

[44] J. T. Costello, E. T. Kennedy, B. F. Sonntag, and C. W. Clark, $3p$ photoabsorption of free and bound Cr, Cr^+, Mn, and Mn^+, Phys. Rev. A **43**, 1441 (1991).

[45] A. D. Shiner, B. E. Schmidt, C. Trallero-Herrero, H. J. Worner, S. Patchkovskii, P. B. Corkum, J. C. Kieffer, F. Legare, and D. M. Villeneuve, Probing collective multi-electron dynamics in xenon with high-harmonic spectroscopy, Nat. Phys. **7**, 464 (2011).

[46] V. Strelkov, Role of autoionizing state in resonant high-order harmonic generation and attosecond pulse production, Phys. Rev. Lett. **104**, 123901 (2010).

[47] R. A. Ganeev, T. Witting, C. Hutchison, F. Frank, M. Tudorovskaya, M. Lein, W. A. Okell, A. Zaïr, J. P. Marangos, and J. W. G. Tisch, Isolated sub-fs XUV pulse generation in Mn plasma ablation, Opt. Express **20**, 25239 (2012).

[48] S. Ghimire, A. D. DiChiara, E. Sistrunk, P. Agostini, L. F. DiMauro, and D. A. Reis, Observation of high-order harmonic generation in a bulk crystal, Nat. Phys. **7**, 138 (2011).

[49] G. Vampa, C. R. McDonald, G. Orlando, D. D. Klug, P. B. Corkum, and T. Brabec, Theoretical analysis of high-harmonic generation in solids, Phys. Rev. Lett. **113**, 073901 (2014).